A new semiempirical model of Saturn's bow shock based on propagated solar wind parameters

D. R. Went,[1] G. B. Hospodarsky,[2] A. Masters,[3,4] K. C. Hansen,[5] and M. K. Dougherty[1]

Received 3 December 2010; revised 11 February 2011; accepted 3 April 2011; published 2 July 2011.

[1] A new semiempirical model of Saturn's dayside bow shock is presented. The model uses observations made during the Pioneer 11, Voyager 1, and Voyager 2 flybys as well as data from the first 6 years of the Cassini mission (2004–2010) to derive the average shape of the shock surface and the variation of shock subsolar distance with solar wind dynamic pressure. The 574 bow shock crossings used to construct the model provide good local time coverage of the dayside shock surface up to latitudes of roughly 45°, allowing the three-dimensional shape of the shock surface to be investigated for the first time. Narrowband Langmuir waves observed by the Radio and Plasma Wave Science instrument are combined with propagated solar wind velocities in order to estimate the solar wind dynamic pressure associated with each of the Cassini crossings. An axisymmetric second-order surface is then fit to the resulting crossing distribution, self-consistently accounting for solar wind dynamic pressure variations. The new semiempirical model is compared with existing models of Saturn's bow shock and magnetopause, and the physical implications of the model are discussed. On the basis of these comparisons, it is proposed that the new semiempirical model is the most accurate representation of Saturn's bow shock surface to date.

Citation: Went, D. R., G. B. Hospodarsky, A. Masters, K. C. Hansen, and M. K. Dougherty (2011), A new semiempirical model of Saturn's bow shock based on propagated solar wind parameters, *J. Geophys. Res.*, *116*, A07202, doi:10.1029/2010JA016349.

1. Introduction

[2] Saturn's bow shock was first observed by Pioneer 11 in 1979 [*Smith et al.*, 1980] with subsequent observations being made by Voyagers 1 and 2 in 1980 and 1981 and Cassini from 2004 onward. Some of the early Cassini observations were studied in detail by *Achilleos et al.* [2006], who, in agreement with previous studies by *Smith et al.* [1980], found the dayside bow shock to have a predominately quasi-perpendicular geometry with a well developed foot, overshoot and ramp [*Burgess*, 1995]. The ramp was found to have a typical thickness of the order of an ion inertial length (at Saturn, ≈1000 km) while the instantaneous velocity of the shock surface, which moves in response to changes in the size and shape of the magnetospheric cavity, was estimated to be 10–100 km s^{-1}. Further studies by *Bertucci et al.* [2005] revealed nonlinear waves in the foreshock region upstream of the bow shock while *Masters et al.* [2008, 2009] reported the first evidence of hot flow anomalies [*Schwartz et al.*, 2000] near the shock surface. More recently, *Clarke et al.* [2010] identified a 1–2 R_S oscillation in the position of the shock (with a period close to that of Saturn's rotation) interpreted as a response to the oscillating magnetopause first reported by *Clarke et al.* [2006].

[3] Studying the global shape and dynamics of the bow shock offers important insights into the physics governing its formation. At large distances from the planet, gas dynamic theory predicts a geometry known as the Mach cone with a flaring angle inversely proportional to the magnetosonic Mach number of the upstream solar wind [*Slavin et al.*, 1984]. Closer to Saturn, the shape of the shock is intimately related to that of the magnetospheric obstacle. *Kanani et al.* [2010] describe the magnetopause using a dynamic pressure-dependent, axisymmetric model but higher-order departures from this symmetry are probable. At Jupiter, for example, *Huddleston et al.* [1998] have confirmed a persistent "polar flattening" of the magnetopause associated with the equatorial magnetodisk [*Smith et al.*, 1974] while *Mühlbachler et al.* [2004] find that the terrestrial magnetopause moves closer to the planet when dayside reconnection (resulting from oppositely directed planetary and interplanetary magnetic fields) is occurring. Higher-order bow shock structure and dynamics may also be associated with variations and asymmetries in the upstream solar wind. *Peredo et al.* [1995], for example, studied the second-order structure and dynamics of the terrestrial bow shock and find dependencies on both solar wind Alfvenic Mach number and interplanetary magnetic field orientation. Such asymmetries are reviewed

[1]Blackett Laboratory, Imperial College London, London, UK.
[2]Department of Physics and Astronomy, University of Iowa, Iowa City, Iowa, USA.
[3]Centre for Planetary Sciences, University College London/Birkbeck, London, UK.
[4]Mullard Space Science Laboratory, Department of Space and Climate Physics, University College London, Dorking, UK.
[5]Space Research Building, University of Michigan, Ann Arbor, Michigan, USA.

0148-0227/11/2010JA016349

for the inner planets by *Slavin and Holzer* [1981] and may also be present at Saturn.

[4] In this paper we study the average shape of Saturn's bow shock as well as the response of this surface to changes in the dynamic pressure of the upstream solar wind. To do this, a functional form is chosen to describe the geometry of the shock surface and the parameters of this function are adjusted until the model gives the best possible fit to the observed distribution of bow shock crossings and their corresponding solar wind dynamic pressures. The solar wind dynamic pressure is difficult to determine during the Cassini era due to pointing constraints associated with the Cassini Plasma Spectrometer [*Young et al.*, 2004] and the lack of a dedicated upstream solar wind monitor at Saturn. As a result, Cassini era dynamic pressures are instead estimated from near-Earth solar wind velocity measurements [*Zieger and Hansen*, 2008] and Langmuir waves observed upstream of the bow shock by the Cassini Radio and Plasma Wave Science (RPWS) instrument *Gurnett et al.* [2004]. The functional form of the model and the mathematical techniques used to determine the optimal parameters vary from one publication to another, as do the methods used to account for such things as trajectory biasing, surface waves and the scatter introduced by variable solar wind dynamic pressure. These methods are reviewed by *Slavin and Holzer* [1981] and used, in conjunction with the extensive bow shock observations now available at Saturn, to produce (in section 4) what we believe to be the most accurate functional form describing Saturn's dayside bow shock surface to date.

2. Existing Empirical Models

[5] We begin by discussing the empirical model of *Slavin et al.* [1985], constructed using Pioneer 11 and Voyager observations. The location of bow shock crossings in the KSM coordinate system (defined such that x_{KSM} is in the solar direction, z_{KSM} is in the plane formed by x_{KSM} and the Saturnian magnetic dipole axis, and y_{KSM} completes the orthogonal set) were rotated such that the solar wind flow direction is antiparallel to the KSM x axis, thus defining the so-called aberrated KSM coordinate system. This rotation, typically less than 2° at Saturn, compensates for an apparent aberration in the solar wind velocity vector (in the rest frame of the planet) caused by Saturn's 9.7 km s^{-1} mean orbital velocity about the Sun. Crossings observed within 10 hours of each other were then averaged together in order to avoid biasing the model toward intervals containing a large number of closely spaced crossings of the shock. A second-order surface, axisymmetric about the solar wind flow direction, was then fit to the spatial location of 7 averaged bow shock crossings. Such a surface may be described by the equation of a conic section:

$$r = \frac{L}{1 + \epsilon \cos\theta}, \tag{1}$$

where $\theta = \cos^{-1}(x/r)$ is the polar angle, r is the radial distance from the focus position to the shock surface, and L is the semi latus rectum. In this formalism the eccentricity, ϵ, describes how blunt or streamlined the shock surface is with $\epsilon < 1$ implying an ellipsoidal surface, $\epsilon = 1$ a paraboloidal surface and $\epsilon > 1$ a hyperboloidal surface.

[6] The semi latus rectum of the best-fitting conic section was then varied such that the model surface intersected each of the 7 observed bow shock crossings in turn. For each intersection, the value of r corresponding to $\theta = 0$ (the shock subsolar distance, R_{SN}) was extracted from the model and plotted against the corresponding upstream solar wind dynamic pressure, P_{DYN}. The shock subsolar distance was then found to vary with the upstream solar wind dynamic pressure as $R_{SN} = 13.33P_{DYN}^{-1/5.1}$ where distances are expressed in units of Saturn radii (R_S = 60268 km) and pressures in units of nanopascals. This relationship was used to normalize the radial distance of each bow shock crossing to the mean solar wind dynamic pressure of the data set. Another axisymmetric surface was then fit to the pressure-normalized distribution and found to have an eccentricity of $\epsilon = 1.71$ and a focus position $x_0 = +6\ R_S$ along the aberrated Saturn-Sun line. Hereafter, this model will be referred to as S85.

[7] *Hendricks et al.* [2005] constructed their bow shock around the empirical magnetopause model of *Maurice and Engle* [1995]. The shape of the shock surface is defined by the shock subsolar distance and, at large distances downstream of the planet, the asymptotic Mach cone angle. The former parameter is obtained from the relationship between shock subsolar distance and the magnetopause subsolar standoff distance and radius of curvature proposed by *Petrinec and Russell* [1997]. This model, hereafter referred to as H05, is well described by a conic section with a focus position at the center of the planet. The associated eccentricity is $\epsilon = 1.02$ and the shock subsolar distance scales with dynamic pressure as $R_{SN} = 13.17P_{DYN}^{-1/5.8}$ [*Achilleos et al.*, 2006]. This makes the H05 model significantly less flared and slightly more resistant to changes in the upstream solar wind dynamic pressure than that of S85.

[8] Using a similar technique to S85, *Masters et al.* [2008] fit a conic section, constrained such that the focus position is at the center of the planet, to 163 aberrated bow shock crossings observed in Saturn's morning-side environment near the equatorial plane. The majority of these crossings were made by Cassini (between June 2004 and August 2005) but, for these crossings, solar wind dynamic pressure measurements were not readily available as discussed in section 1. The solar wind density associated with each crossing was instead estimated from Cassini RPWS observations of narrowband Langmuir waves upstream of the bow shock. This density was combined with a constant solar wind speed of 500 ± 100 km s^{-1} and used to estimate the upstream solar wind dynamic pressure with a ≈40% uncertainty. The shock subsolar distance was found to vary with solar wind dynamic pressure as $R_{SN} = 14P_{DYN}^{-1/6}$ but the power law constant in this expression had a large (≈30%) relative uncertainty. *Masters et al.* [2008] therefore assumed the same power law constant found by *Arridge et al.* [2006] for the magnetopause (4.3 ± 0.3) and, upon fitting a new conic section to the pressure-normalized set of crossings, found a marginally hyperbolic bow shock well described by an eccentricity of $\epsilon = 1.05$. This model is hereafter referred to as M08A.

[9] To improve the quality of their model *Masters et al.* [2008] returned to the unnormalized set of bow shock crossings. The mean solar wind velocity and the two parameters describing the scaling of the shock subsolar distance with solar wind dynamic pressure were then set as additional

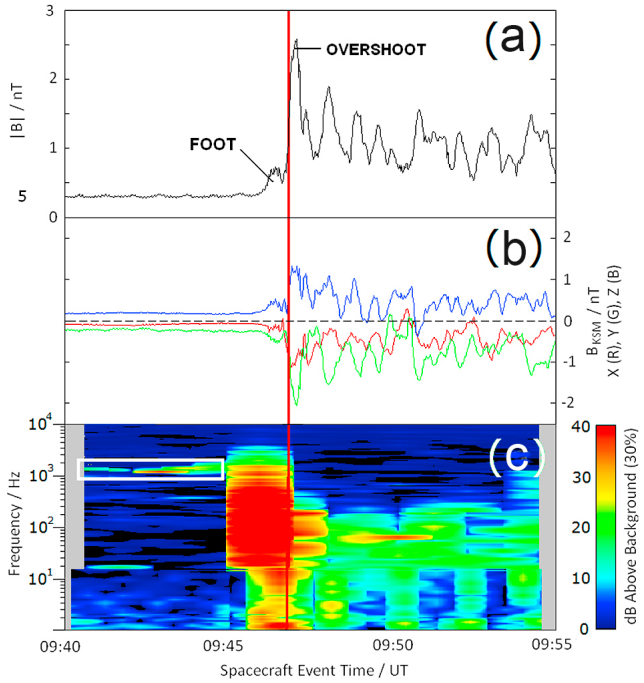

Figure 1. Cassini magnetometer (MAG) and Radio and Plasma Wave Science (RPWS) data for a 15 min interval surrounding a quasi-perpendicular crossing of Saturn's bow shock made by Cassini on 27 June 2004. (a) Magnetic field magnitude. (b) Three Kronocentric Solar Magnetospheric (KSM) magnetic field components. (c) RPWS spectrogram with narrowband Langmuir waves (surrounded by a white box) observed upstream of the bow shock at a frequency of roughly 1500 Hz. The intense, broadband noise observed by RPWS at about 0945 UT is evidence of Cassini encountering the bow shock, while the point of transition (used to construct the model) is denoted by a red line.

free parameters in the model and the optimal conic section was recalculated. The result, hereafter referred to as the M08B model, was a more streamlined bow shock (with an eccentricity of $\epsilon = 0.92$) with the optimized parameters suggesting a mean solar wind velocity of 700 km s^{-1}. This velocity is outside the range observed by *Crary et al.* [2005] and prompted the authors to prefer the original M08A construction.

3. Observations

[10] We consider data from all four spacecraft to visit the Saturnian system to date. Bow shock crossings made prior to August 2005 have already been identified and were used by *Slavin et al.* [1985] and *Masters et al.* [2008] in the construction of their empirical models. To identify bow shock crossings made by Cassini after August 2005, data from the dual-technique magnetometer [*Dougherty et al.*, 2004] was considered. Figure 1 shows the first inbound bow shock crossing observed by Cassini on 27 June 2004. Figure 1a shows the magnetic field strength as a function of time, Figure 1b shows the corresponding components in the KSM coordinate system and Figure 1c shows a frequency-time spectrogram recorded by the Cassini Radio and Plasma Wave Science instrument [*Gurnett et al.*, 2004] over the same interval. The magnetic field in the upstream solar wind is generally low in magnitude and constant in direction (over the 15 min time scale under consideration) while the magnetosheath field is generally stronger and more variable. The bow shock forms the transition between these two regimes, denoted by a red line in Figure 1. In the RPWS frequency-time spectrogram, Langmuir waves (an intense, narrow band emission surrounded by a white box) can be seen upstream of the bow shock while, at the point of crossing itself, an intense broadband noise is associated with currents flowing within the shock surface.

[11] The sharpness of the transition in Figure 1 and the presence of a well defined shock foot and overshoot (labeled) is typical of the supercritical, quasi-perpendicular geometry encountered by Cassini [*Achilleos et al.*, 2006]. For some crossings however, a less distinct quasi-parallel geometry was observed and the transition between the solar wind and magnetosheath was more gradual. Such a crossing, made on 14 July 2004, is shown in Figure 2 in the same format as Figure 1. In these cases the approximate center of the solar wind-to-magnetosheath transition (denoted by a red line in Figure 2) is adopted as the shock location. The temporal uncertainty in identifying the transition time (estimated by eye) is typically less than 60 s and does not

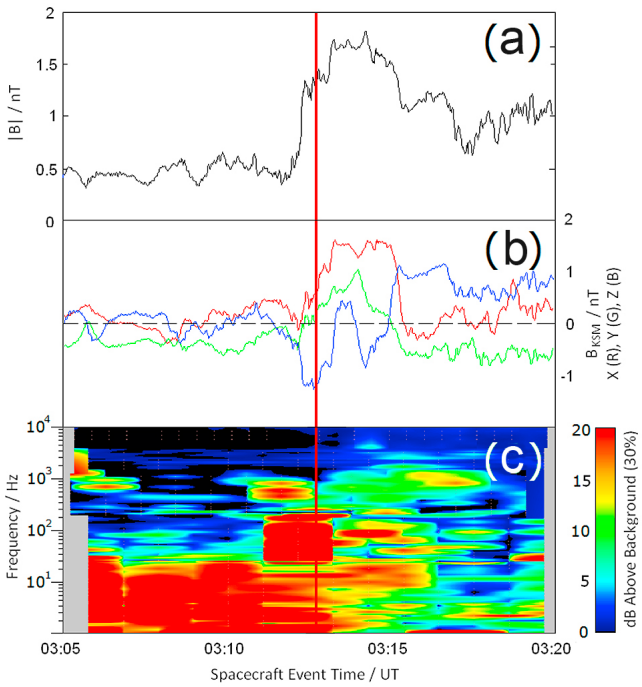

Figure 2. Cassini MAG and RPWS data for a 15 min interval surrounding a quasi-parallel crossing of Saturn's bow shock made by Cassini on 14 July 2004. (a) Magnetic field magnitude. (b) Three KSM magnetic field components. (c) RPWS spectrogram with narrowband Langmuir waves (surrounded by a white box) observed upstream of the bow shock at a frequency of roughly 700 Hz. The intense, broadband noise observed by RPWS at about 0312 UT is evidence of Cassini encountering the bow shock, while the point of transition (used to construct the model) is denoted by a red line.

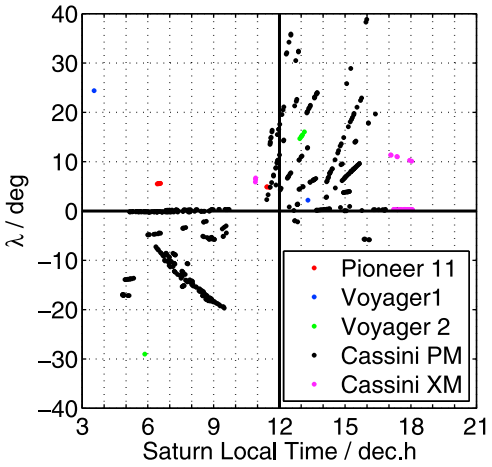

Figure 3. The local time and latitudinal distribution of all 574 bow shock crossings observed at Saturn between August 1979 and July 2010. Crossings were made by Pioneer 11 (red circles), Voyager 1 (blue circles), and Voyager 2 (green circles) and during the Cassini Prime (solid circles) and Extended (magenta circles) missions.

exceed 10 min for any crossing. This corresponds to a spatial distance of less than 0.1 R_S, a figure well within the RMS spread of the model presented in section 4 and insignificant when compared with the spatial scale of the shock surface (several R_S) under consideration.

[12] In this study we consider 574 crossings of Saturn's bow shock made between August 1979 and July 2010. The spatial distribution of these crossings is shown in Figure 3 with Saturn local time (SLT) on the x axis and planetocentric latitude, λ, on the y axis. The crossings are evenly distributed between 0600 and 1800 SLT and extend poleward to planetocentric latitudes of up 40°. This represents a significant improvement over the S85 and M08A/B distributions, both of which were restricted to low latitudes in the prenoon (0600 < SLT < 1200) quadrant.

[13] Direct measurements of the solar wind density and velocity were made upstream of each pre-Cassini bow shock crossing (in order to estimate the upstream solar wind dynamic pressure) however such measurements are typically unavailable in the Cassini era. For these crossings the upstream solar wind density was instead estimated from the frequency of narrowband Langmuir waves observed upstream of the bow shock by the Cassini RPWS instrument [*Gurnett et al.*, 2004]. These waves are clearly visible in Figures 1c and 2c, where they appear (surrounded by a white box) as a narrow band of increased power, centered at approximately 1500 Hz and 700 Hz, upstream of the crossing. Within this band the frequency, f_L, at which the wave intensity reaches a maximum is proportional to the square root of the electron number density, n_e, of the plasma medium through which the waves are propagating:

$$f_L \approx 8980\sqrt{n_e}, \tag{2}$$

where f_L is expressed in hertz and n_e per cubic centimeter. A quasi-neutral solar wind composed of 4% helium and 96% hydrogen (by number [*Bame et al.*, 1977]) was then assumed in order to arrive at the solar wind mass density. *Crary et al.* [2005] found a highly variable solar wind near Saturn and, to account for this variability, only the average Langmuir frequency observed within 7 min upstream of each bow shock crossing was used in this investigation. Langmuir waves observed further from the bow shock than this may not be representative of the solar wind density (and hence dynamic pressure) at the time of the crossing itself. An identical averaging window was used in the construction of the M08A and M08B models and, although the choice of 7 min was somewhat arbitrary, the parameters of these two models was found to be largely insensitive to reasonable (few minute) variations in the averaging window's size. In addition to this, *Masters et al.* [2008] found that when Langmuir waves were not observed within 7 min of the shock crossing, they were typically not observed for at least an hour upstream of the event.

[14] The solar wind velocity at Saturn was estimated from measurements made near 1AU using the 1.5D MHD solar wind propagation model of *Zieger and Hansen* [2008]. This model predicts the solar wind conditions near Saturn with an uncertainty that is proportional to both the phase of the solar cycle (and hence the amount of small-scale structure in the solar wind) and the relative positions of Saturn, the near-Earth solar wind monitor and the Sun. The temporal uncertainty in the arrival time of a given packet of solar wind plasma at Saturn was taken into account by using, for each crossing, the average propagated velocity observed within a narrow temporal window centered on the time of each crossing. The width of this window (32 hours on average) was related to the time since (apparent) opposition via the functional form derived by *Zieger and Hansen* [2008] for the conditions of high solar wind recurrence index appropriate to the Cassini era solar minimum. Solar wind propagations are available for the entirety of the Cassini prime mission (2004–2008) but are not yet available for the Equinox extension. The solar wind velocity associated with the 30 Equinox bow shock crossings was therefore set equal to the mean solar wind velocity associated with all 544 earlier encounters with the bow shock. With an uncertainty defined by the standard deviation of the data set, this mean velocity is 448 ± 47 km s^{-1}. By not assuming a constant solar wind velocity for the vast majority of Cassini era bow shock crossings, the uncertainty in the upstream solar wind dynamic pressure estimates has been significantly reduced when compared with the earlier modeling of M08A and M08B.

[15] Upstream solar wind dynamic pressures could be either measured or estimated for 330 (57%) of the 574 bow shock crossings observed at Saturn during the period of interest. For the remaining 244 bow shock crossings, no Langmuir waves were observed within the predefined 7 min window and, as a result, a reasonable estimation of the associated upstream solar wind plasma density was impossible.

[16] Constructing an unbiased model using these 330 crossings is associated with a number of important caveats. Firstly, variations in spacecraft trajectory and velocity can change the number of bow shock crossings observed in a given region of space independently of upstream solar wind dynamic pressure variations. This may bias the model toward intervals with an artificially large number of bow shock crossings such as times when the Cassini trajectory was parallel to the mean location of the bow shock. The

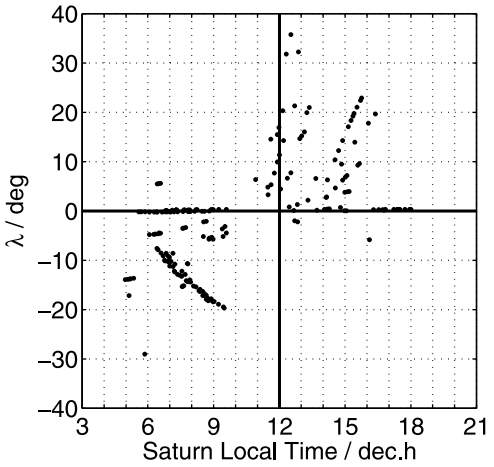

Figure 4. Local time and latitudinal distribution of the 203 averaged bow shock crossings used in the construction of the new semiempirical model.

second caveat is that, for constant solar wind dynamic pressure, surface waves (such as those inferred by *Clarke et al.* [2010]) may result in oscillations of the shock position about the mean location. These oscillations may introduce artificial "noise" into the optimization procedure and reduce the quality of the fit. S85 attempted to address both problems by averaging together any bow shock crossings observed within 10 hours of each other and we employ a similar methodology here by averaging together bow shock crossings observed in consecutive 10 hour windows. For each of the "averaged" bow shock crossings in the new data set, the mean distance between the constituent (unaveraged) bow shock crossings was calculated along with the mean upstream solar wind dynamic pressure and its standard deviation. The average value of the mean distance between constituent bow shock crossings was found to be 0.6 R_S (maximum value = 3.7 R_S) while the standard deviation of the solar wind dynamic pressure was typically less than 15% (and never greater than 98%) of the mean.

[17] It is possible that the mean shape of Saturn's bow shock exhibits a seasonal variation related to changes in Saturn's magnetospheric configuration [*Arridge et al.*, 2008]. Empirical models of the shock surface may then be biased toward the seasonal period during which most of the bow shock crossings were made. In total, roughly 89% of the 574 crossings used in the construction of this model were made during "southern summer" conditions for which the solar latitude, θ_{SUN}, exceeded 8°. Just 10% of crossings were made during "equinocturnal" conditions ($|\theta_{\mathrm{SUN}}| < 8°$) while only 1% were made during "northern summer" conditions for which $\theta_{\mathrm{SUN}} < -8°$. The asymmetry of this distribution prevents us from investigating seasonal variations in shock shape and position at this time however, should such variations exist, it is clear that the results presented in the following sections will be strongly biased toward the "southern summer" configuration.

[18] A final consideration is that, in the downstream limit discussed in section 2, the shape of the bow shock is determined by the asymptotic Mach cone angle and not the shape of the magnetospheric obstacle. Since we are interested in studying the shape dayside bow shock surface only, crossings associated with an x-axis coordinate < -24 R_S were excluded from further consideration before the temporal averaging was performed. For reference, 24 R_S is the mean distance to the subsolar magnetopause determined by *Achilleos et al.* [2009] and, as a result, is approximately equal to one obstacle radius. The resulting data set, consisting of 203 averaged bow shock crossings, is shown in Figure 4. In Figure 4, SLT is plotted on the x axis and planetocentric latitude, λ, on the y axis. The averaged crossings are well distributed across the low- to midlatitude dayside shock surface and are used to construct the new semiempirical model of Saturn's bow shock presented in section 3.

4. The New Semiempirical Model

[19] In this section the new semiempirical model of Saturn's bow shock is presented. Owing to the lack of bow shock crossings at high ($\lambda > 70°$) latitudes, it is useful to begin modeling the shock under the assumption of axisymmetry about the solar wind flow direction, as in the previous modeling efforts discussed in section 2. Working in aberrated KSM coordinates and constraining the focus of the conic section to lie at the center of the planet, the shock subsolar distance, R_{SN}, is the radial distance to the shock surface when the polar angle, θ, in equation 1 is set to zero:

$$R_{\mathrm{SN}} = \frac{L}{1+\epsilon}. \tag{3}$$

This distance is assumed to vary with dynamic pressure, P_{DYN}, according to an as yet unknown power law of the form

$$R_{\mathrm{SN}} = c_1 P_{\mathrm{DYN}}^{-1/c_2}, \tag{4}$$

where c_1 and c_2 are parameters to be determined. Substituting equations (3) and (4) into equation (1) allows us to express the size and shape of the bow shock in terms of the parameters c_1, c_2, and ϵ:

$$r = \frac{(1+\epsilon)c_1 P_{\mathrm{DYN}}^{-1/c_2}}{1+\epsilon\cos\theta}. \tag{5}$$

[20] In this formulation the shape of the bow shock surface is held constant (for a given set of parameters) but its size is allowed to vary self-similarly with the upstream solar wind dynamic pressure. The optimum value of parameters c_1, c_2, and ϵ was determined using a nonlinear least squares technique in which the root mean square (RMS) difference between the predicted and observed radial distance to the aberrated bow shock crossings was minimized using an optimization routine based on the *Nelder and Mead* [1965] simplex algorithm. The uncertainty in the resulting parameters was estimated using a Monte Carlo method, similar to that of *Arridge et al.* [2006] and *Masters et al.* [2008], in which the fitting described above was repeated 200 times. At each iteration the fit was carried out using 80% of the total number of crossings (chosen at random) and the standard deviation of the resulting distribution of each optimized parameter was taken as the uncertainty in that parameter.

[21] The result of this minimization procedure, shown in Figure 5, is a shock surface with an eccentricity of $\epsilon \approx 0.84$

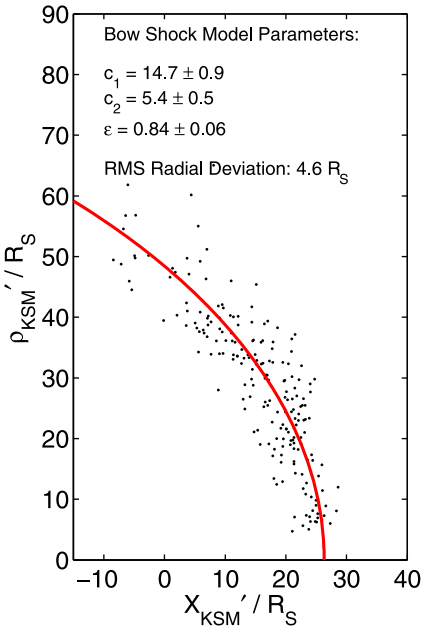

Figure 5. The new semiempirical model of Saturn's bow shock (red) with the pressure-corrected distribution of the 203 averaged bow shock crossings (obtained using the new model power law) in the aberrated KSM x-ρ plane.

and a subsolar distance which scales with the upstream solar wind dynamic pressure as $R_{SN} = 15P_{DYN}^{-1/5.4}$. The associated RMS radial deviation of the fit was 4.6 R_S. The fit was recalculated using 5 and 15 hour averaged crossings, completely unaveraged crossings and crossings which had been spatially averaged by grouping together all crossings made within the same 1 R_S^3 volume of a 200 × 200 × 200 R_S grid. The parameters thus obtained were identical to those presented here to within the statistical resolution of the data sets in question indicating that the method of data averaging does not significantly bias the resulting model. A similar result was found when the initial parameters used for iteration were varied within reasonable ($0 < c_1 < 1000$, $0.5 < c_2 < 100$, $0 < \epsilon < 5$) bounds.

5. Higher-Order Structure and Dynamics

[22] The model described above is a first-order approximation only and higher-order departures from this picture are predicted by a number of different theories and simulations including those of *Walters* [1964], *Cloutier* [1976], and *Ogino et al.* [1988]. The improved spatial coverage of the bow shock crossings utilized in this study allows some of these predictions to be tested at Saturn for the first time.

[23] General departures from axisymmetry can be investigated by fitting a higher-order functional form to the aberrated crossing distribution used in section 3. Following the methodology of *Formisano* [1979], a general second-order surface is assumed:

$$0 = a_1 + a_2X + a_3Y + a_4Z + a_5XY + a_6YZ + a_7XZ + a_8X^2 + a_9Y^2 + a_{10}Z^2, \quad (6)$$

with the value of the constants a_4, a_6 and a_7 set to zero in order to force the resulting surface to be symmetric about the aberrated x-y plane. This makes it easier to constrain the surface to a crossing distribution which has no high-latitude ($\lambda > 70°$) observations while still allowing departures from axisymmetry to be investigated. These asymmetries may include a difference in the mean distance to the bow shock along the dawn and dusk terminators as well as a difference in the mean "width" of the shock along the aberrated KSM y and z axes. Introducing additional free parameters to describe the dynamic pressure dependence of this surface makes the resulting model difficult to constrain with the available observations. Instead, in order to reduce the noise associated with different solar wind dynamic pressures, the radial distance of each crossing in the aberrated KSM system was normalized to the mean solar wind dynamic pressure of the data set (0.045 nPa) using the power law derived in section 4 before the new fit was attempted:

$$r_N = r\left(\frac{P_{DYN}}{\langle P_{DYN}\rangle}\right)^{1/5.4}, \quad (7)$$

where r_N is the normalized radial distance to the crossing. No departures from axisymmetry were present to within the statistical resolution of the data set and the focus location of the axisymmetric conic section best describing the resulting surface was found to be within errors of the center of the planet.

[24] Another way to investigate higher-order bow shock structure and dynamics is to compare the parameters of axisymmetric fits made using multiple independent subsets of bow shock crossings. Such an approach, utilizing a separate set of high- and low-latitude crossings, was used by *Huddleston et al.* [1998] to study the three-dimensional shape of the Jovian shock surface. Applying the same methodology to Saturn reveals no evidence for either dawn-dusk asymmetries or polar flattening (within the errors of the resulting model parameters) and a similar null result was obtained when bow shock crossings were organized by solar wind dynamic pressure and interplanetary magnetic field orientation. Attempts to introduce additional free parameters to the axisymmetric model of section 4 typically found that either the shape and location of the bow shock was independent of the new parameter (within the errors of the parameter) or that the optimization routine failed to converge on a physically realistic solution.

[25] The above findings suggest that, on average, the axisymmetric bow shock model assumed in section 4 is a good first-order approximation to the true Saturnian bow shock. The apparent lack of higher-order structure and dynamics may be due to of the comparatively low number of bow shock crossings utilized by this study in comparison with the very large (>1300 crossings) data sets used by authors such as *Peredo et al.* [1995] at the Earth. Uncertainties in the estimation of the upstream solar wind dynamic pressure associated with each individual crossing of the bow shock may also be responsible. However the asymmetries in question may also be smaller and hence harder to detect at Saturn due to the higher magnetosonic Mach number of the solar wind, the transitory nature of Saturn's magnetodisk [*Arridge et al.*, 2008] and the larger radius of curvature of the magnetodisk at Saturn compared with Jupiter [*Achilleos et al.*, 2009]. No attempt to investigate the dependence of bow shock position and shape on the

Table 1. Empirical (and Semiempirical) Models of Saturn's Dayside Bow Shock

Model	Crossings (Averaged)	ϵ	x_0	c_1	c_2	RMS (New Data Set)
S85	13 (7)	1.71	6 R_S	13.33 R_S	5.1	11.5 R_S
H05	N/A (N/A)	1.02	0 R_S	13.17 R_S	5.8	6.1 R_S
M08A	163 (N/A)	1.05 ± 0.09	0 R_S	12.3 ± 0.7 R_S	4.3 ± 0.3[a]	5.7 R_S
M08B	163 (N/A)	0.92 ± 0.08	0 R_S	17 ± 1 R_S	5.7 ± 0.5	7.3 R_S
New model	329 (203)	0.84 ± 0.06	0 R_S	15 ± 1 R_S	5.4 ± 0.5	4.6 R_S

[a]Assumed to be equal to that of the *Arridge et al.* [2006] magnetopause model.

solar wind magnetosonic or Alfvenic Mach numbers was made in this study due to the difficulty involved in determining the solar wind temperature associated with the large number of bow shock crossings made by Cassini.

6. Discussion

[26] The shapes predicted by the new and existing models of Saturn's bow shock (Table 1) are shown in Figure 6 for a common shock subsolar distance of 28 R_S. Note that this common subsolar distance does not correspond to a common solar wind dynamic pressure but does serve to illustrate the differences in bow shock shapes between the different models which, in Figure 6, are shown projected on to the aberrated KSM x-ρ plane. Model S85 (green) is clearly the most eccentric of the five while the eccentricities of the remaining models are similar. The dependence of shock subsolar distance on solar wind dynamic pressure is presented separately in Figure 7 where solar wind dynamic pressure (measured in nanopascals) runs along the x axis and shock subsolar distance (measured in R_S) runs along the y axis. Both axes have logarithmic scaling and the mean and standard deviation of the solar wind dynamic pressure distribution are labeled.

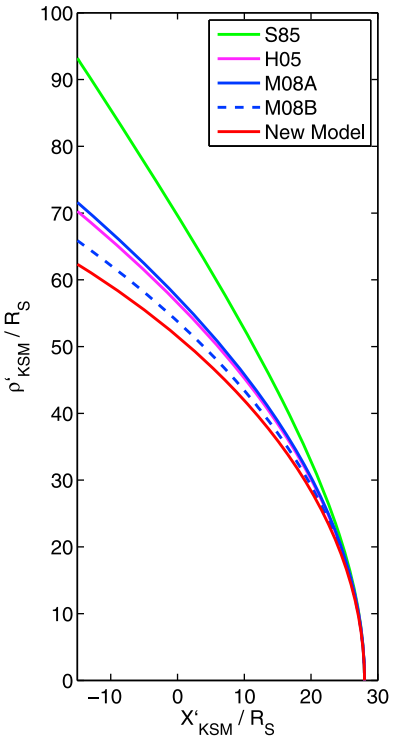

Figure 6. Bow shock shapes for S85 (green line), H05 (magenta line), M08A (blue line), M08B (blue dashed line), and the new semiempirical model (red line). In each case, the shock subsolar distance, R_{SN}, has been normalized to 28 R_S.

[27] The low eccentricity of the new semiempirical model, shown in red in Figure 6, gives it the most streamlined geometry of all bow shock models released to date and is significantly more streamlined than the hyperbolic model of S85, shown in green. The new eccentricity is, however, within errors of both the M08A and M08B values. The shock subsolar distance is found, in this study, to vary with solar wind dynamic pressure as $R_{SN} = 15P_{DYN}^{-1/5.4}$ with previous models having power law constants ranging from c_2 = 4.3 (M08A) to c_2 = 5.9 (H05). With reference to Figure 7, it is clear that, for a given solar wind dynamic pressure, the new model (red line) predicts a larger shock subsolar distance than any of the existing models with the exception of M08B (blue dashed line) and, at low dynamic pressures, M08A (blue line). On the basis of the new model and the 574 bow shock crossings observed at Saturn so far, the mean shock subsolar distance is found to be approximately 28 R_S with a standard deviation of 4 R_S.

[28] It is useful to investigate the statistical validity of the new model by comparing it with those discussed in section 2.

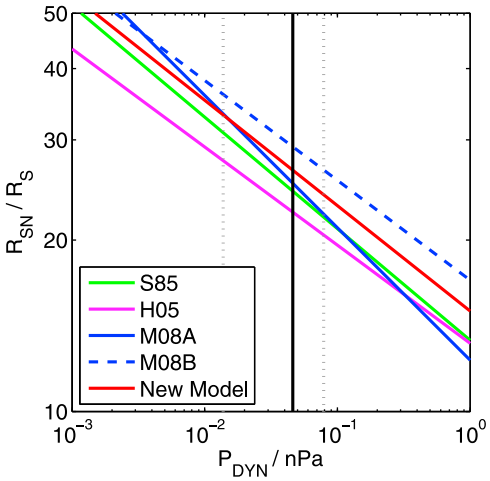

Figure 7. Variation of bow shock subsolar distance, R_{SN}, with solar wind dynamic pressure, P_{DYN}, for S85 (green line), H05 (magenta line), M08A (blue line), M08B (blue dashed line), and the new semiempirical model (red line). The mean solar wind dynamic pressure (0.045 nPa) is denoted by a vertical solid line, while the shaded dotted lines represent 1 standard deviation to either side of this mean.

To do this the RMS radial deviation between each of the existing models and the 203 averaged bow shock crossings used in constructing the new semiempirical model was calculated and compared. The smallest RMS radial deviation was associated with the new semiempirical model, as expected, followed in turn by M08A (RMS = 5.7 R_S), H05 (RMS = 6.1 R_S), M08B (RMS = 7.3 R_S) and S85 (RMS = 11.5 R_S). The ordering and approximate RMS of these models was found to be insensitive to the method used to average the observed bow shock crossings and, on this basis, it is proposed that the new semiempirical model, with its more streamlined shape and moderate response to solar wind dynamic pressure variations, represents the most accurate form of Saturn's bow shock surface to date.

[29] As expected, the new bow shock surface is more flared than the *Kanani et al.* [2010] magnetopause for the full range of solar wind dynamic pressures for which these models are both valid. In addition to this, the scaling of shock subsolar distance with solar wind dynamic pressure is found to be in good agreement with the scaling found for the *Kanani et al.* [2010] magnetopause. Although the shock subsolar distance is not required to scale with the upstream solar wind dynamic pressure in exactly the same way as the magnetopause, the motion of the magnetopause is expected to be the dominant contributor to bow shock motion, as discussed in section 1, and consequently our results suggest that both models are estimating the solar wind dynamic pressure (and associated boundary scaling) with a reasonable degree of accuracy. Combining the *Kanani et al.* [2010] magnetopause model with the new semiempirical bow shock model presented in this paper, and considering a mean solar wind dynamic pressure of 0.045 nPa, the subsolar bow shock to magnetopause ratio is found to be 1.3 ± 0.3 while the corresponding subsolar magnetosheath thickness is poorly constrained at 6 ± 4 R_S.

[30] The scaling of the bow shock subsolar distance with solar wind dynamic pressure is intermediate between Jupiter [*Huddleston et al.*, 1998] and the Earth [*Slavin and Holzer*, 1981] which, on the basis of empirical studies, have power law constants of roughly 4 and 6, respectively. These figures reflect the compressibility of each planet's magnetosphere since it is the motion of the magnetopause that most strongly influences the position of the shock. The observed ordering suggests that, while plasma pressure and centrifugal forces in the outer magnetosphere have an appreciable effect on Jupiter's magnetospheric compressibility, the effect may not be as significant at Saturn and is even less important at the Earth. It is interesting to compare this idea with recent observational studies of Saturn's ring current [*Sergis et al.*, 2010] and with semiempirical models of both Jupiter and Saturn's magnetodisks [*Achilleos et al.*, 2009]. While these studies support our general conclusion that internal pressure plays an important role in determining the structure and dynamics of Saturn's magnetosphere and magnetopause, they also highlight the complicated relationship that exists between the different sources of internal magnetospheric pressure and the subsolar location of the magnetopause and bow shock. Further studies of this relationship are likely to fruitful areas of research.

[31] The theoretical value of the subsolar bow shock to magnetopause ratio at Saturn [*Slavin et al.*, 1985] is of the order of 1.6, somewhat larger than the value of 1.3 ± 0.3 inferred from the new bow shock and magnetopause models but still within the quoted level of uncertainty. A thinner subsolar magnetosheath may be the result of plasma flowing away from the equatorial plane and over the poles of the planet, as would be expected if the magnetopause was more streamlined in the noon-midnight(as opposed to equatorial) plane due to the presence of an equatorial magnetodisk. Flattening of the Jovian magnetopause has been confirmed by *Huddleston et al.* [1998] but more robust conclusions with regards to Saturn await the study of higher latitude magnetopause crossings (currently in progress) and a further reduction in the uncertainty of both boundaries scaling with solar wind dynamic pressure. The ratio of subsolar bow shock to magnetopause distance at Saturn is intermediate between (but within errors of) the Jovian and terrestrial values of 1.2 and 1.41 obtained by *Huddleston et al.* [1998] and *Slavin and Holzer* [1981], respectively.

[32] The new semiempirical model is significantly less flared than its Jovian equivalent with the shock eccentricity $\epsilon = 0.84 \pm 0.06$ being much smaller than the dayside values of $\epsilon = 1.05$ and $\epsilon = 1.1$–1.2 found for Jupiter by *Slavin et al.* [1985] and *Huddleston et al.* [1998]. The *Huddleston et al.* [1998] study failed to find any evidence of polar flattening in the average shape of the Jovian bow shock (despite evidence for such being observed in the magnetopause) in line with the results for Saturn's bow shock presented in this paper.

7. Summary

[33] A new semiempirical model of Saturn's dayside bow shock has been presented. The model is axisymmetric about the solar wind flow direction and is well described by the following equation:

$$r = \frac{(1+\epsilon)c_1 P_{\mathrm{DYN}}^{-1/c_2}}{1+\epsilon\cos\theta}, \tag{8}$$

with constants $c_1 = 15 \pm 1$, $c_2 = 5.4 \pm 0.5$ and $\epsilon = 0.84 \pm 0.06$. In this formalism the upstream solar wind dynamic pressure, P_{DYN}, is measured in units of nanopascals while the position of an arbitrary point on the shock surface is given by the coordinates (r, θ). Here r is the radial distance from Saturn to the bow shock (measured in units of Saturn Radii, R_S = 60,268 km) while the polar angle $\theta = \cos^{-1}(x/r)$ where x is the projection of r onto the Saturn-Sun line, equivalent to the KSM x-axis coordinate. The model is valid for solar wind dynamic pressures of 0.003–0.2 nPa, latitudes of $|\lambda| < 40°$ and aberrated x-axis positions less than 24 R_S downstream of the planet. On the basis of a comparison between this model and existing models of the bow shock it is proposed that the new semiempirical model presented in this paper is the most accurate representation of Saturn's dayside bow shock surface to date. This is primarily a result of the large number of bow shock crossings used in the construction of the model and the use of propagated solar wind velocities to estimate the upstream solar wind dynamic pressure associated with each crossing. No asymmetries in the shape of the bow shock surface could be resolved in our observations and no evidence for the shock shape and subsolar distance being dependent on the properties of the solar wind (with the exception of the upstream solar wind

dynamic pressure) was found. The new semiempirical model suggests that the scaling of the magnetopause subsolar standoff distance with solar wind dynamic pressure is intermediate between that observed at Jupiter and the Earth, consistent with the results of recent modeling of Saturn's magnetopause.

[34] **Acknowledgments.** The authors would like to thank J. Cutler and S. Kanani for their assistance in compiling the list of Cassini-era bow shock crossings used in this investigation. D.R.W. was supported by a U.K. STFC postgraduate studentship at Imperial College London. Additional support was received from U.K. STFC through rolling grants to MSSL/UCL and Imperial College London.

[35] Philippa Browning thanks James F. Carbary and another reviewer for their assistance in evaluating this manuscript.

References

Achilleos, N., et al. (2006), Orientation, location, and velocity of Saturn's bow shock: Initial results from the Cassini spacecraft, *J. Geophys. Res.*, *111*, A03201, doi:10.1029/2005JA011297.

Achilleos, N., P. Guio, and C. S. Arridge (2009), A model of force balance in Saturn's magnetodisc, *Mon. Not. R. Astron. Soc.*, *401*, 2349–2371, doi:10.1111/j.1365-2966.2009.15865.x.

Arridge, C. S., N. Achilleos, M. K. Dougherty, K. K. Khurana, and C. T. Russell (2006), Modeling the size and shape of Saturn's magnetopause with variable dynamic pressure, *J. Geophys. Res.*, *111*, A11227, doi:10.1029/2005JA011574.

Arridge, C. S., C. T. Russell, K. K. Khurana, N. Achilleos, S. W. H. Cowley, M. K. Dougherty, D. J. Southwood, and E. J. Bunce (2008), Saturn's magnetodisc current sheet, *J. Geophys. Res.*, *113*, A04214, doi:10.1029/2007JA012540.

Bame, S. J., J. R. Asbridge, W. C. Feldman, and J. T. Gosling (1977), Evidence for a structure-free state at high solar wind speeds, *J. Geophys. Res.*, *82*, 1487–1492, doi:10.1029/JA082i010p01487.

Bertucci, C., N. Achilleos, C. T. Russell, M. K. Dougherty, E. J. Smith, M. Burton, B. T. Tsurutani, and C. Mazelle (2005), Bow shock and upstream waves at Jupiter and Saturn: Cassini magnetometer observations, *Am. Inst. Phys. Conf. Ser.*, *781*, 109–115, doi:10.1063/1.2032682.

Burgess, D. (1995), *Introduction to Space Physics*, Cambridge Univ. Press, New York.

Clarke, K. E., et al. (2006), Cassini observations of planetary-period oscillations of Saturn's magnetopause, *Geophys. Res. Lett.*, *33*, L23104, doi:10.1029/2006GL027821.

Clarke, K. E., D. J. Andrews, A. J. Coates, S. W. H. Cowley, and A. Masters (2010), Magnetospheric period oscillations of Saturn's bow shock, *J. Geophys. Res.*, *115*, A05202, doi:10.1029/2009JA015164.

Cloutier, P. A. (1976), Solar-wind interaction with planetary ionospheres, *NASA Spec. Publ.*, *397*, 111–119.

Crary, F. J., et al.. (2005), Solar wind dynamic pressure and electric field as the main factors controlling Saturn's aurorae, *Nature*, *433*, 720–722, doi:10.1038/nature03333.

Dougherty, M. K., et al. (2004), The Cassini Magnetic Field Investigation, *Space Sci. Rev.*, *114*, 331–383, doi:10.1007/s11214-004-1432-2.

Formisano, V. (1979), Orientation and shape of the Earth's bow shock in three dimensions, *Planet. Space Sci.*, *27*, 1151–1161, doi:10.1016/0032-0633(79)90135-1.

Gurnett, D. A., et al. (2004), The Cassini Radio and Plasma Wave Investigation, *Space Sci. Rev.*, *114*, 395–463, doi:10.1007/s11214-004-1434-0.

Hendricks, S., F. M. Neubauer, M. K. Dougherty, N. Achilleos, and C. T. Russell (2005), Variability in Saturn's bow shock and magnetopause from Pioneer and Voyager: Probabilistic predictions and initial observations by Cassini, *Geophys. Res. Lett.*, *32*, L20S08, doi:10.1029/2005GL022569.

Huddleston, D. E., C. T. Russell, M. G. Kivelson, K. K. Khurana, and L. Bennett (1998), Location and shape of the Jovian magnetopause and bow shock, *J. Geophys. Res.*, *103*, 20,075–20,082, doi:10.1029/98JE00394.

Kanani, S. J., et al. (2010), A new form of Saturn's magnetopause using a dynamic pressure balance model, based on in situ, multi-instrument Cassini measurements, *J. Geophys. Res.*, *115*, A06207, doi:10.1029/2009JA014262.

Masters, A., N. Achilleos, M. K. Dougherty, J. A. Slavin, G. B. Hospodarsky, C. S. Arridge, and A. J. Coates (2008), An empirical model of Saturn's bow shock: Cassini observations of shock location and shape, *J. Geophys. Res.*, *113*, A10210, doi:10.1029/2008JA013276.

Masters, A., et al. (2009), Hot flow anomalies at Saturn's bow shock, *J. Geophys. Res.*, *114*, A08217, doi:10.1029/2009JA014112.

Maurice, S., and I. M. Engle (1995), Idealized Saturn magnetosphere shape and field, *J. Geophys. Res.*, *100*, 17,143–17,152, doi:10.1029/95JA00897.

Mühlbachler, S., V. S. Semenov, H. K. Biernat, N. V. Erkaev, I. V. Kubyshkin, C. J. Farrugia, D. Langmayr, and D. F. Vogl (2004), A reconnection model describing erosion of the magnetopause and the associated bow shock motion, *Adv. Space Res.*, *33*, 2103–2107, doi:10.1016/j.asr.2003.04.052.

Nelder, J. A., and R. Mead (1965), A simplex method for function minimization, *Comput. J.*, *7*, 308–313.

Ogino, T., R. J. Walker, and M. Ashour-Abdalla (1988), A three-dimensional MHD simulation of the interaction of the solar wind with Comet Halley, *J. Geophys. Res.*, *93*, 9568–9576, doi:10.1029/JA093iA09p09568.

Peredo, M., J. A. Slavin, E. Mazur, and S. A. Curtis (1995), Three-dimensional position and shape of the bow shock and their variation with Alfvenic, sonic and magnetosonic Mach numbers and interplanetary magnetic field orientation, *J. Geophys. Res.*, *100*, 7907–7916, doi:10.1029/94JA02545.

Petrinec, S. M., and C. T. Russell (1997), Hydrodynamic and MHD equations across the bow shock and along the surfaces of planetary obstacles, *Space Sci. Rev.*, *79*, 757–791, doi:10.1023/A:1004938724300.

Schwartz, S. J., G. Paschmann, N. Sckopke, T. M. Bauer, M. Dunlop, A. N. Fazakerley, and M. F. Thomsen (2000), Conditions for the formation of hot flow anomalies at Earth's bow shock, *J. Geophys. Res.*, *105*, 12,639–12,650, doi:10.1029/1999JA000320.

Sergis, N., et al. (2010), Particle pressure, inertial force, and ring current density profiles in the magnetosphere of Saturn, based on Cassini measurements, *Geophys. Res. Lett.*, *37*, L02102, doi:10.1029/2009GL041920.

Slavin, J. A., and R. E. Holzer (1981), Solar wind flow about the terrestrial planets: 1. Modeling bow shock position and shape, *J. Geophys. Res.*, *86*, 11,401–11,418, doi:10.1029/JA086iA13p11401.

Slavin, J. A., R. E. Holzer, J. R. Spreiter, and S. S. Stahara (1984), Planetary Mach cones: Theory and observation, *J. Geophys. Res.*, *89*, 2708–2714, doi:10.1029/JA089iA05p02708.

Slavin, J. A., E. J. Smith, J. R. Spreiter, and S. S. Stahara (1985), Solar wind flow about the outer planets: Gas dynamic modeling of the Jupiter and Saturn bow shocks, *J. Geophys. Res.*, *90*, 6275–6286, doi:10.1029/JA090iA07p06275.

Smith, E. J., L. Davis Jr., D. E. Jones, P. J. Coleman Jr., D. S. Colburn, P. Dyal, C. P. Sonett, and A. M. A. Frandsen (1974), The planetary magnetic field and magnetosphere of Jupiter: Pioneer 10, *J. Geophys. Res.*, *79*, 3501–3513, doi:10.1029/JA079i025p03501.

Smith, E. J., L. Davis, D. E. Jones, P. J. Coleman, D. S. Colburn, P. Dyal, and C. P. Sonett (1980), Saturn's magnetic field and magnetosphere, *Science*, *207*, 407–410, doi:10.1126/science.207.4429.407.

Walters, G. K. (1964), Effect of oblique interplanetary magnetic field on shape and behavior of the magnetosphere, *J. Geophys. Res.*, *69*, 1769–1783, doi:10.1029/JZ069i009p01769.

Young, D. T., et al. (2004), Cassini Plasma Spectrometer Investigation, *Space Sci. Rev.*, *114*, 1–112, doi:10.1007/s11214-004-1406-4.

Zieger, B., and K. C. Hansen (2008), Statistical validation of a solar wind propagation model from 1 to 10 AU, *J. Geophys. Res.*, *113*, A08107, doi:10.1029/2008JA013046.

M. K. Dougherty and D. R. Went, Blackett Laboratory, Imperial College London, London SW7 2AZ, UK. (daniel.went08@imperial.ac.uk)

K. C. Hansen, Space Research Building, University of Michigan, Ann Arbor, MI 48109, USA.

G. B. Hospodarsky, Department of Physics and Astronomy, University of Iowa, Iowa City, IA 52242, USA.

A. Masters, Mullard Space Science Laboratory, Department of Space and Climate Physics, University College London, Dorking RH5 6NT, UK.